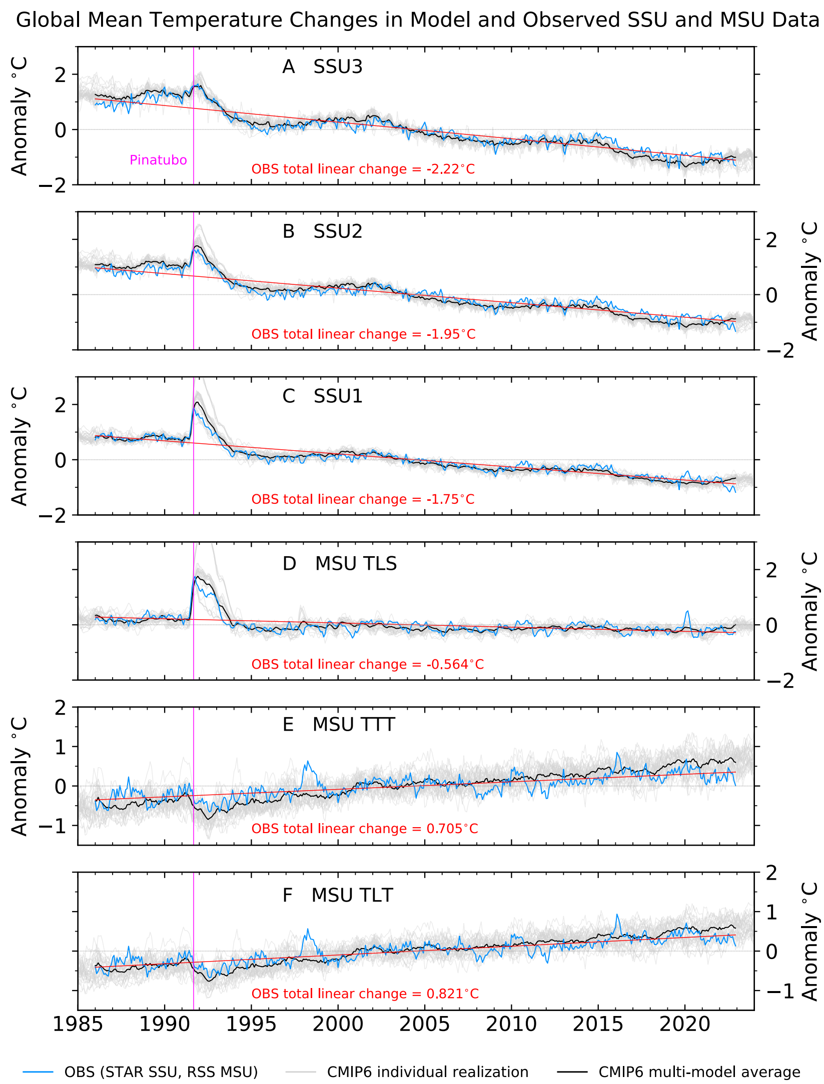

Fig. 1. Observed and simulated changes in global-mean monthly mean temperature in six atmospheric layers. Results are temperatures from channels 3, 2, and 1 of the Stratospheric Sounding Unit (SSU; panels *A–C*) (27), lower stratospheric temperature from the Microwave Sounding Unit (MSU TLS; panel *D*), MSU total tropospheric temperature (TTT; panel *E*), and MSU lower tropospheric temperature (TLT; panel *F*) (25). The peaks of the weighting functions for these six layers are at *ca.* 45, 38, 30, 19, 5.6, and 3.1 km above the Earth's surface (respectively). Results are anomalies relative to climatological monthly means over 1986 to 2022. Model simulations are from nine different CMIP6 models and a total of 32 realizations of historical climate change (*Methods* and *SI Appendix*).

ozone depletion and ozone recovery (respectively) (28, 45); the fourth period has substantially larger net anthropogenic forcing than the first. As in Fig. 2, control run trend distributions provide information on the magnitude of unforced atmospheric temperature changes. This information is valuable for assessing the significance of the forced temperature trends in the $HIST_{ext}$ simulations.

Consider the troposphere first. In TLT and TTT, each successive 25-y period has larger ensemble-mean tropospheric warming and greater separation from the mean of the sampling distribution of unforced trends (i.e., higher S/N levels). This progressive warming is consistent with increasing positive forcing by anthropogenic greenhouse gases. The early 1950 to 1974 period has large, time-increasing negative anthropogenic sulfate aerosol forcing (49), which helps to explain why the ensemble-mean $HIST_{ext}$ tropospheric temperature trends over this period are close to zero. Anthropogenic sulfate aerosol forcing decreases nonlinearly in the three subsequent analysis periods (49, 50), yielding a decrease in sulfate aerosol-induced tropospheric cooling. Although these pronounced temporal changes in anthropogenic sulfate aerosol forcing influence TLT and TTT, they have minimal effect on simulated stratospheric temperature trends.

In the three SSU channels, stratospheric cooling occurs in each of the four analysis periods and in every $HIST_{ext}$ realization (Fig. 3 *A–C*). As in the case of the 1986 to 2022 period, cooling in the $HIST_{ext}$ runs amplifies with increasing height and is invariably significantly larger than 25-y trends arising from internal variability. One key difference relative to the tropospheric results in Fig. 3 *E* and *F* is that stratospheric cooling does not increase monotonically as the 25-y analysis window advances. The effect of the large stratospheric ozone depletion over 1975 to 1999 is to augment CO_2-induced stratospheric cooling. As a result, the ensemble-mean $HIST_{ext}$ cooling of each SSU channel (and of TLS) is larger over 1975 to 1999 than in the subsequent 2000 to 2024 period. By 2025 to 2049, the primarily CO_2-driven cooling of the S_{25-50} layer exceeds the CO_2 and ozone-driven S_{25-50} cooling over 1975 to 1999.

Fig. 3 shows that despite important changes over time in the relative contributions of ozone and GHG forcing, the